JOURNAL OF GEOPHYSICAL RESEARCH, VOL. 105, NO. B9, PAGES 21,633–21,646, SEPTEMBER 10, 2000

Mount Etna dense array local earthquake P and S tomography and implications for volcanic plumbing

Mireille Laigle, Alfred Hirn, Martine Sapin, and Jean-Claude Lépine
Laboratoire de Sismologie Expérimentale, Département de Sismologie, UMR 7580 CNRS
Institut de Physique du Globe, Paris

Jordi Diaz and Josep Gallart
Institut de Ciencies de la Terra "Jaume Almera," Consejo Superior de Investicagiones Científicas
Barcelona, Spain

Rinaldo Nicolich
Dipartimento di Ingegneria Navale del Mare i per l'Ambiente, Università di Trieste, Trieste, Italy

Abstract. Inversion for the three-dimensional velocity structure of Mount Etna is performed with a data set of arrival times of P and S waves of local earthquakes from temporary dense arrays of three-component seismographs. A high-V_p body revealed by the original tomography without nearby stations is confirmed, and its image is sharpened using new velocity constraints provided by refraction data. Synthetic tests of V_p and V_p/V_s and comparison with an independent artificial source tomography with a fundamentally different geometry consistently calibrate the significance threshold of the resolution indicators. The trustworthy part of the image shows a high-V_p body centered under the southern part of Valle del Bove above the 6 km below sea level deep basement, which extends towards sea level and may be rooted in or through the crust. It has a large contrast of over 1 km/s with the surrounding sediments and sharp lateral limits and can thus be regarded as made of intrusive material of magmatic origin. The massive high-V_p body is heterogeneous in V_p/V_s. The regions inside it where V_s is relatively low can then be suspected of containing a proportion of melt or be fractured and act as pressure links or transport zones. Such features may be structurally linked and appear to be activated in eruptive phenomena. By taking into account the heterogeneities in structure and physical state retrieved by seismic tomography a succession of seismic events, deformational episodes, and geochemical variation in lavas can be discussed with respect to the well-observed eruptions.

1. Introduction

In an attempt to bring an image of Mount Etna (Figure 1a) into focus we carried out a comprehensive survey with several seismic methods at different scales and resolutions [*Hirn et al.*, 1997; *Laigle*, 1998]. This huge active basaltic volcano is in an unusual location. In map view, it is south and in front of the subduction zone marked by the slab dipping northward beneath the Calabrian block. On an E-W cross section from the Ionian marine basin to northeastern Sicily, it is at the edge of the Mesozoic passive continental margin. Marine reflection seismic profiles reveal active normal faults, as well as heterogeneities in lithospheric structure, inherited from the Mesozoic evolution of the passive margin to the Ionian Sea, with which they interact [*Nicolich et al.*, 2000]. These results could suggest that the development of Etna volcano is structurally related and coeval with features in the lithosphere that indicate a recent change [*Hirn et al.*, 1997]. The slab of Ionian lithosphere to the NNW, under the Calabrian arc and Tyrrhenian Sea, is still identified by seismicity and velocity structure [*Selvaggi and Chiarabba*, 1995]. Half a million years ago, the regime at the surface changed from regional compression toward the Calabrian arc to extension in the region SE of Etna. This change was presumably controlled by a change in coupling at the interplate boundary. It may result from the stranding of the Sicilian-Peloritan block against the Hyblean continental promontory of Africa, while the slab of Ionian oceanic material under the Tyrrhenian continues its rollback. Etna appears to be constructed uphill of the lateral edge of this slab, defined from seismicity in the mantle under the Tyrrhenian Sea. A crustal-scale active, normal fault at sea continues this direction from Etna toward the SSE, oblique to the Malta Escarpment of the Mesozoic paleomargin [*Hirn et al.*, 1997; *Nicolich et al.*, 2000]. These active tectonic features at sea are suggested to be sources of the two major catastrophic earthquakes of 1169 and 1693 in eastern Sicily. These seismic events then appear structurally linked to Etna. They also appear to follow the two major changes in eruptive style and magma discharge rate over the millennium, with a third one being in progress [*Hirn et al.*, 1997].

Across Etna, the variation of the deep lithospheric structure is resolved from offshore-onshore crustal refraction and teleseismic data, with which former data [*Sharp et al.*, 1980] can be consistently interpreted in terms of a mantle upwarp. At its top, magma may pond under the crust, but a large amount of

Paper number 2000JB900190.
0148-0227/00/2000JB900190$09.00

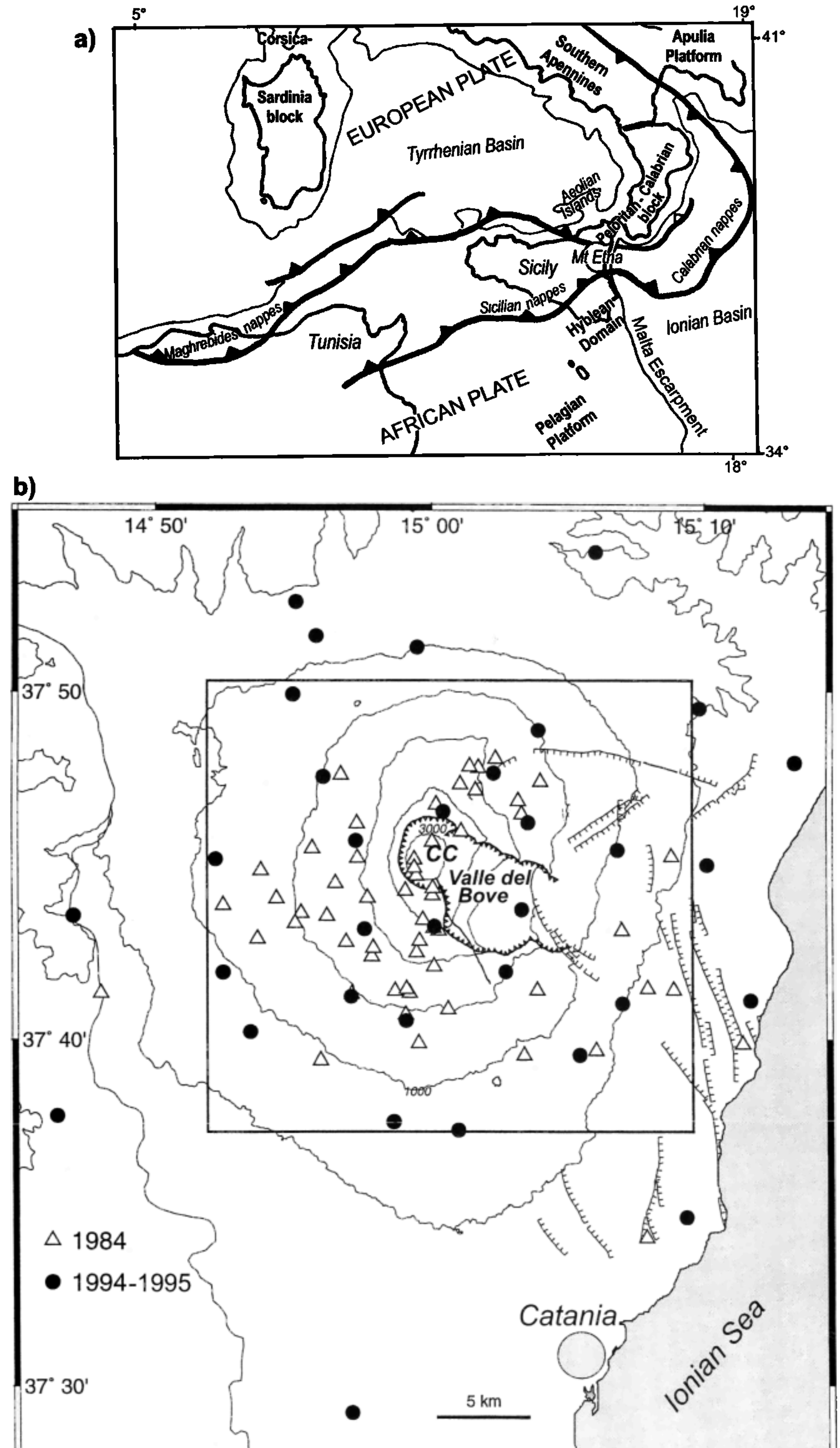

Figure 1. (a) Geological framework of Mount Etna volcano in the central Mediterranean region, adapted from *Catalano et al.* [1996]. (b) Location map of temporary seismic arrays on Etna, eastern Sicily, Italy, of principally three-component instruments deployed in 1984 (open triangles) and in 1994 and 1995 (solid circles). The box encompasses the region shown in subsequent figures displaying inversion results. Elevation contours are every 500 m. Normal faults are indicated with barbs. The curved barbed line includes the Valle del Bove horseshoe depression of the upper eastern flank and the Central Craters (CC) to its northwest.

it may not erupt and instead may be advected sideways in the present lithospheric-scale extension and related asthenospheric upwelling, as is the case under oceanic spreading centers [*Hirn et al.*, 1997]. This allows reconciliation of discrepancies in the interpretation of some petrological or geochemical observations, which appear when such a huge magma chamber is assumed to be trapped inside the crust. At a smaller scale a body characterized by a high velocity of P waves, or high-V_p

body, previously detected in the crust under the edifice by local earthquake tomography [*Hirn et al.*, 1991] can now be shown, with an artificial source restricted-ray tomography [*Laigle and Hirn*, 1999], to reach a shallow level. Exsolution of SO_2, whose rate of discharge at Etna is exceptional, much higher than expected from the eruption rate, can only occur at shallow depth [*Allard*, 1997]. Since the high-V_p body reaches such a shallow depth, it can be made of the magma from which the gas is exsolved. This magma is not erupted and returns to freeze at depth, its storage being eased by the extensional regime [*Laigle and Hirn*, 1999].

Velocity tomography from travel times of local earthquakes is developing as a method for retrieving the three-dimensional (3-D) internal structure of volcanoes, thus providing elements for understanding their plumbing system and the geological evolution of their edifice. Eruption-feeding conduits, geothermally altered regions, magma chambers, and solidified magmatic intrusions have been detected by a number of studies of other volcanoes. In subduction-related volcanoes, smaller volumes of high V_p and also less massive low-V_p structures (the latter regarded as conduits) have been detected, e.g., at Redoubt, Alaska [*Benz et al.*, 1996]; Unzen, Japan [*Ohmi and Lees*, 1995]; and Mount St. Helens [*Lees and Crosson*, 1989; *Lees*, 1992]. Large high-V_p bodies are commonly found and interpreted as solidified intrusions, as, for instance, Hengill-Grensdalur central volcano, Iceland [*Toomey and Foulger*, 1989]; Mauna Loa and Kilauea and their rift zones [*Okubo et al.*, 1997] and Kilauea volcano, Hawaii [*Thurber*, 1984; *Rowan and Clayton*, 1993; *Dawson et al.*, 1999]; and Piton de la Fournaise, Réunion Island [*Nercessian et al.*, 1996]. For these volcanoes built near oceanic spreading centers or by the action of plumes on oceanic plates, these intrusions within the edifice are part of a broader process which also builds their substructure, oceanic plate, or oceanic island. At Etna the volcanic edifice itself is small and constructed on preexisting continental crust covered by thick sedimentary layers. We suggested that the intrusive material can find space to form this large high-V_p body not only within the edifice but under it, within the preexisting sedimentary volume and possibly deeper in the crust as a consequence of the recent regime of lithosperic extension evidenced on the regional scale [*Hirn et al.*, 1997; *Nicolich et al.*, 2000].

In the present paper we investigate the fine structure of the intracrustal intrusive magmatic body beneath Etna with high-resolution seismic tomography. In a first experiment of local earthquake tomography (LET) on Mount Etna volcano in 1984, we used a dense temporary array (Figure 1b) including stations on the upper slopes and summit craters, with mostly three-component seismographs [*Hirn et al.*, 1991]. Tightly constrained hypocenters allowed insight into earthquake distribution in space and time [*Nercessian et al.*, 1991]. These *P* and *S* data were inverted iteratively but without ray tracing through the updated models [*Hirn et al.*, 1991]. The main structural feature suggested by this tomography was a high-V_p body embedded in the pre-Etnean sediments which reached from sea level down to 6 km below sea level (bsl). This has since been confirmed by refraction-reflection profiles [*Accaino et al.*, 1998; *Laigle et al.*, 1998]. Subsequent LET studies have principally used the sparser array with mostly vertical component stations of the permanent volcano monitoring stations [*Cardaci et al.*, 1993; *De Luca et al.*, 1997; *Villaseñor et al.*, 1998]. In the results the location, shape, and size of this high-V_p body were only partly recovered. However, we have now confirmed that this high-V_p body indeed reaches up to a shallow depth inside the thick sedimentary cover, with an artificial source undershooting experiment that considers rays propagating only above the basement [*Laigle and Hirn*, 1999]. In order to improve the original LET, dense arrays of up to 35 stations with three-component seismographs were again deployed during two 5–6 week periods in 1994 and 1995 (Figure 1b). Seismic activity was rather low, and only 20% additional data were provided. The new data provide a significant check of the earlier experiment since the array was broader, sites were different, and, in particular, seismographs could be located closer to the high-V_p body, including one in the rough Valle del Bove, which had never been instrumented before. New refraction results contribute to defining the initial 1-D model. With the augmented database we perform a number of synthetic tests to assess the reliability of the image, so that anomalies in V_p/V_s can also be discussed. We propose tentative interpretations of some of these anomalies and suggest that corresponding structures have been activated in the major complex eruptions of Etna 1989 and 1991–1993 and allow interpretation of some of its specific features.

2. Reference 1-D Velocity Model and 3-D Inversion

In seismic tomography the 3-D model of *P* and *S* wave velocity heterogeneity can be inferred by an iterative inversion procedure linearized with respect to a reference 1-D model of velocity versus depth. Hence the 3-D results depend on the 1-D reference model chosen. In local earthquake tomography (LET) this reference model, termed the "minimum 1-D model," can be computed with the arrival time data set according to the procedure outlined by *Kissling et al.* [1994]. However, this procedure is already a linearized inversion and hence depends on an initial model which has to be defined as a first step of the forward problem. In the present case, we constrain this initial model, independent from the LET data, by taking into account the refraction seismic lines from diverse shot points around and on the volcano [*Accaino et al.*, 1998; *Laigle et al.*, 1998]. The refraction velocity values thus measured from sea level down to 6 km bsl appear >0.5 km s^{-1} higher than those used in the reference models of the original tomography [*Hirn et al.*, 1991] and subsequent ones, as displayed in Plate 1d. In the new initial 1-D model we used the first arrival refraction velocities but increased the values toward the base of the sedimentary cover to take into account gradients common in these layers. This increase is nevertheless conservative, since the refraction lines sample mostly the surroundings of the high-V_p plug, and hence the velocities that they provide are still lower than the areal average.

However, in the volcanic edifice itself the velocity-depth function is not constrained independently, and several initial models need to be tested against the LET data. Among them, two end-member models are discussed further: initial model G, for gradient (red in Plate 1d), has a velocity-depth increase from the summit to 2 km bsl, whereas model C, for constant, has a constant velocity from the summit to 1 km bsl (dark blue, with red underneath in Plate 1d). Both models, even the latter one, are discretized into 0.5-km-thick layers in order to allow the 1-D minimum procedure to use the data to perturb this constant velocity. The two minimum 1-D models resulting from these two different initial models differ in detail but show two important common features: a contrast in velocity from

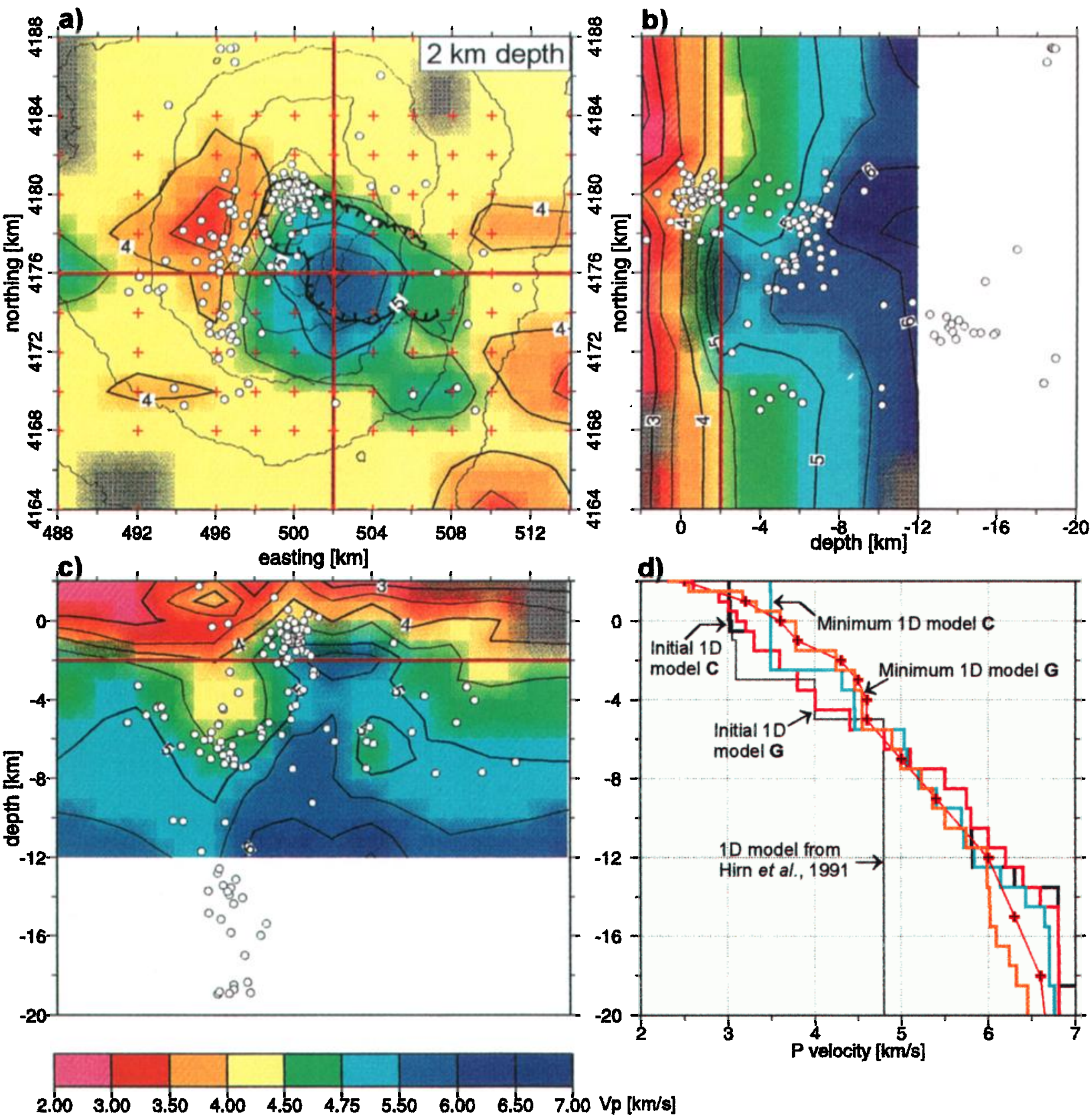

Plate 1. *P* wave velocity model resulting from the tomographic inversion, isolines every 0.5 km s^{-1}, kilometric UTM coordinate system. (a) Map at 2 km bsl, (b) N-S section at km 502 E, (c) E-W sections at km 4176 N, and (d) velocity-depth functions as discussed in text: initial and minimum 1-D of two models G and C for the present inversion and model of *Hirn et al.* [1991]. Red crosses mark nodes of the 3-D inversion scheme in plane in Plate 1a and in depth in Plate 1d.

above to below 2 km bsl and a major, deeper velocity contrast at roughly the same depth of 5.5 km bsl. Moreover, the information in the LET data has brought the velocities to higher values in the shallow part of the model, consistent with the refraction results. Residuals in the hypocentral locations have a rather large root-mean-square (RMS) value, which is not attributable to inaccurate data, since timing and reading resolution are of the order of 0.01 s. In the minimum 1-D inversion this results in large station terms. These terms have, however, consistent values over broad areas encompassing stations of the three different surveys and are not therefore related to local problems of instrument type or site geology. They are to be taken as due to structure, and the 3-D inversion shall be allowed to retrieve it. For this 3-D inversion the gradient model G is preferred. The reason is that it relocates as shallower those earthquakes that are associated with eruptive phenomena recorded at the surface in October 1984 and October 1996. The results of the 3-D tomography displayed in the following have to be considered with respect to this minimum 1-D model G (red in Plate 1d).

For the 3-D inversion we use a data set of 156 well-observed earthquakes with an average of 21 data per event, totaling 3319 observations, 2130 of *P* and 1189 of *S* waves. Here we consider our whole dense array data set including 1984, 1994, and 1995 and use the inversion code SIMULPS of *Thurber* [1983], *Eberhart-Phillips* [1993], and *Kissling* [1988], modified by *Thurber* [1993] and *Evans et al.* [1994]. This code has also been used in tomographies of Etna by *Cardaci et al.* [1993] and *De Luca et al.* [1997]. It considers the joint problem of earthquake location and propagation in a heterogeneous model of both V_p and V_p/V_s fields, and it solves the problem iteratively by using a damped least squares method. Travel times are computed at each iteration in a medium interpolated among a 3-D array of nodes with the updated velocity values, using an approximate ray tracer with a pseudo-bending method [*Um and Thurber*, 1987]. The new results concerning the high-V_p body do agree with those obtained earlier by *Hirn et al.* [1991]. This is noteworthy because the previous code was based on a model parametrization with blocks of constant velocity and did not take into account the modification of the structure when retracing the rays from one iteration to the other.

To adapt to the numbers of data and unknowns, we choose a 2-km spacing of nodes in horizontal planes (red crosses in Plate 1a) and 1-km spacing down to 5 km bsl and then at 7, 9, and 12 km bsl (red crosses on velocity-depth function in Plate 1d). All computations have been made with two grids rotated 45° with respect to each other. Results are displayed in the common N-S, E-W frame but have all been checked to also appear in the other inversions and hence to be independent of grid orientation. To avoid overinterpreting the data, we present the results of an inversion with rather conservative parameters, such as a damping of 10 s^2 km^{-1} chosen from synthetic tests discussed in section 3. After three iterations the variance is reduced by 75%, and the RMS residual is reduced from 0.36 s to 0.18 s.

3. Three-Dimensional V_p Tomographic Results and Synthetic Tests of Significance of V_p and V_p/V_s

On the *P* wave velocity deviation map at 2 km bsl (Plate 1a) a large high-V_p region is found centered on the southern Valle del Bove. Its western edge is particularly sharp and separates large domains. A lateral velocity contrast up to 30% corresponds to the well-known pre-Etnean sediments, with a velocity of around 4 km s^{-1}. The sediments surround a core with high velocity, up to 5.5 km s^{-1}, which is likely made of intrusive material of magmatic nature. Such a strong and sharp lateral contrast embedded in the sediments is also obvious in the wide-angle reflection-refraction profiles of the controlled-source survey [*Laigle and Hirn*, 1999]. A first indication of the trustworthiness of this main feature is that it had been found with a completely different inversion code and initial model [*Hirn et al.*, 1991]. A second indication can be derived from the analysis of the ray sampling. Also, in order to estimate the reliability of results, synthetic model reconstruction tests for the specific source-receiver geometry of observation have been proposed [*Humphreys and Clayton*, 1988; *Spakman et al.*, 1989]. The commonly used checkerboard tests essentially illustrate the spatial sampling and resolution of the ray geometry but do not test the reliability of large-scale structure [*Lévèque et al.*, 1993], such as the one found here. Hence we prefer to test synthetic models which have structures of large size and of high amplitude. This also helps to define the value of the parameters to be used for the inversion of observed data, for example, a damping factor of 10 s^2 km^{-1}, which allows a compromise between the recovery of the amplitude and the spatial smoothing of the anomalies. For synthetic models we will first consider a high-V_p bar, with a geometry different from the result of the inversion of observations. Then we will consider a cube mimicking the upper part of these results, and finally, we will consider synthetic models that take the V_p structure resulting from the inversion of observations but two different hypotheses for the corresponding V_p/V_s structures. For each test we compute times between the source and receiver locations of the real experiment, through the synthetic model, invert them, and compare the result to the model. Since the high-V_p domain appears bounded by a N-S limit in the west (Plate 1a and Figure 2a), we consider a synthetic model that instead extends as an E-W bar with a 20% positive anomaly (Figure 2b). This model is reasonably retrieved by the test (Figure 2c). Hence the N-S oriented boundary resulting from the inversion of the observed data is a trustworthy feature required by the observations, not an artifact due to inadequate ray geometry, assumptions, inversion code, or parameters, which are the same for the synthetic and observed data.

The distribution in space of the reliability of the image can be displayed by mapping indicators of the quality of the data, such as hit count and derivative weight sum, or resulting from the inversion, such as the resolution matrix. Parameters extracted from the full-resolution matrix, such as the value of the diagonal element and the spread function [e.g., *Menke*, 1984], have been discussed by *Toomey and Foulger* [1989]. Their distribution indicates the relative quality of results through the model. However, the threshold value of the indicators, below which images should be disregarded, depends on the particular experiment geometry and inversion parameters in a nonexplicit way, and there is no simple means to estimate this threshold value. Synthetic tests allow definition of the regions where the model can be reconstructed adequately. The resolution indicators can then be calibrated by identifying their value in these regions of acceptable results. In the present case, the inversion of the synthetics of the high-V_p bar appears to retrieve the model correctly inside the inner contour in Figure 2c, which is that part of space where the diagonal term of the resolution matrix has a value in excess of 0.05 and where the resolution spread function has values smaller than 1.2. Inside the outer contour (values of 1.5 for the spread function), nodes are still moderately well resolved, but outside results should be discarded. Results are not commonly thought of as being significant down to a value of the diagonal term as small as calibrated here. For the resolution spread function, however, the threshold value is relatively small, even better than those commonly considered. This reflects the fact that the absolute values themselves have no strong meaning, which is well known, since they depend on characteristic details of the inversion, for instance, the number of parameters, as discussed by *Toomey and Foulger* [1989]. When we use a sparser gridding or do not compute V_p/V_s, the diagonal term increases to values found for other tomographies. This is, of course, at the cost of a loss in model fidelity as recalled by *Toomey and Foulger* [1989], which is obviously not justified here since it implies losing V_p/V_s. In the following, the structures inside the 1.2 or at least 1.5 value contours of the spread function are discussed.

An even stronger proof, independent from the synthetic tests, that establishes the threshold of significance of resolution parameters in the present particular LET of Etna is presented by *Laigle and Hirn* [1999]. It is based on the comparison of the

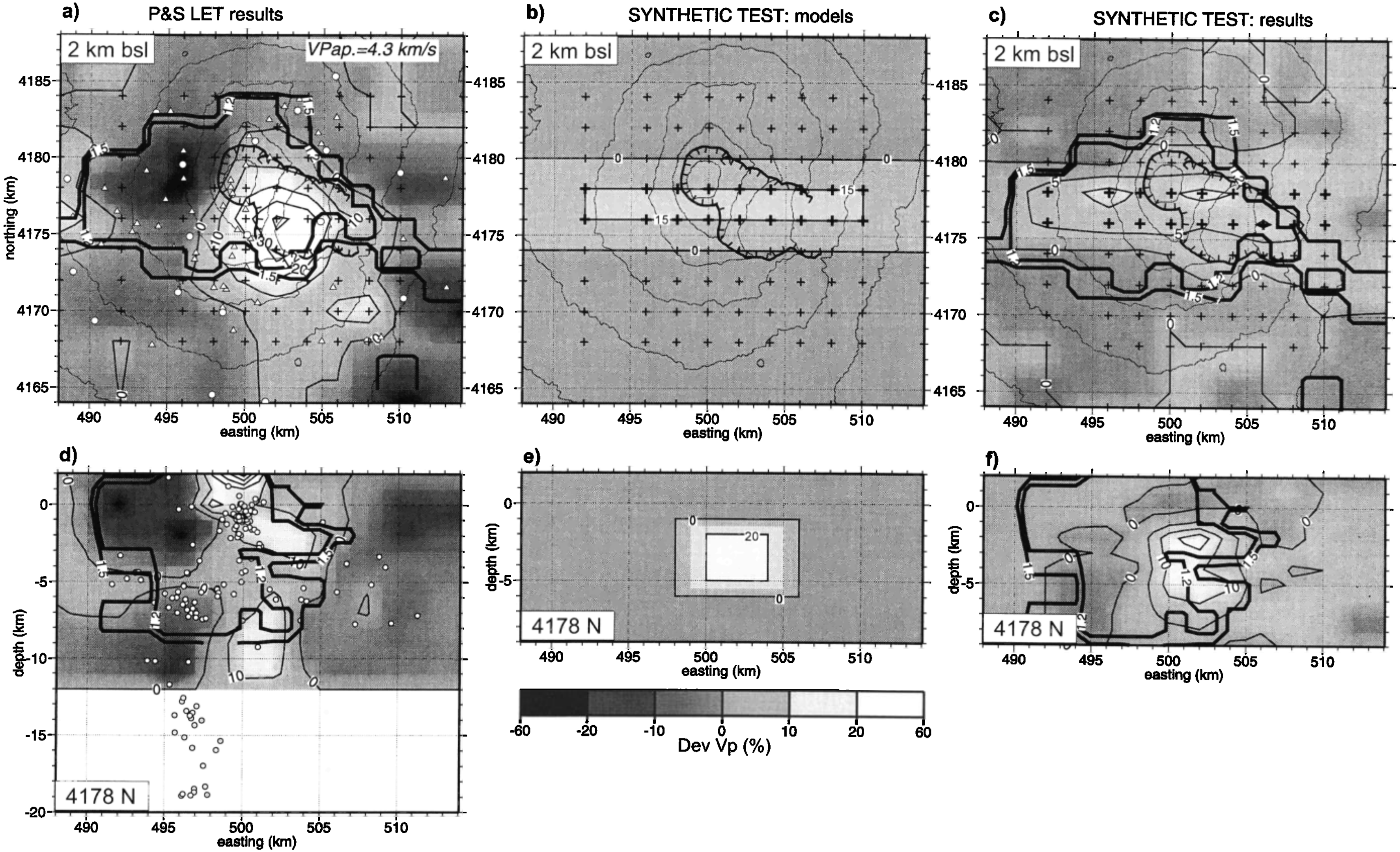

Figure 2. From left to right, results of the inversion of observations, models, and results of inversion of their synthetics. Contours superimposed on results are for values of the resolution indicators extracted from the full resolution matrix. Inner contour is the value of 0.05 for the diagonal term as calibrated by the comparison with results of artificial source tomography [*Laigle and Hirn*, 1999]. This same inner contour corresponds to a value of 1.2 for the resolution spread function. Outer contour is 1.5 for the spread function, above which results are not reliable. Maps at 2 km bsl of (a) V_p deviation (in %) resulting from the inversion of observed data, (b) the synthetic model of E-W bar of high V_p over 2 km thickness centered at 2 km bsl, and (c) result of the inversion of these synthetics to be compared with model in Figure 2b. East-west sections at 4178 N of (d) V_p deviation (in %) resulting from the inversion of observed data, (e) the synthetic model of a cube, centered 1 km south of the section, and (f) the result of the inversion of synthetics to be compared to model in Figure 2e to estimate recovery and leakage.

LET results with those of an artificial source tomography experiment (RAST, for Restricted ray Artificial Source Tomography) with completely different geometries and wave types, which has been specifically designed and carried out for this purpose in the experimental effort on Mount Etna. In the RAST experiment, borehole shots at diverse azimuths from the summit of Etna were recorded on the opposite side. The geometry, with the source at the surface and the short shot-receiver distance, restricts the waves recorded as first or early arrivals corresponding to rays reflected or refracted above the basement interface at 6 km bsl. In this upper volume, within the regions well sampled by the two independent tomographies, RAST and LET can then be considered to have resolved the structure reliably where they give the same result and not reliably where their results differ. The limit between these two parts of the space [*Laigle and Hirn*, 1999] allows calibration of the threshold value of parameters extracted from the resolution matrix results. The value of 1.2 for the spread function found with the results of the present LET synthetic test is consistent with this different approach.

On vertical cross sections of V_p through the Valle del Bove (Plates 1b and 1c and Figure 2d) the high-V_p body is seen to reach through the whole upper 5–7 km and confirms the original result of the first tomography of Etna of *Hirn et al.* [1991]. Its 5-km-diameter core has a velocity over 5.5 km s^{-1}, contrasting with a velocity lower by 1–1.5 km s^{-1} in the surrounding sediments. At its edge the isolines of the absolute value of the velocity are vertical. This is orthogonal to the assumed horizontal layering of any reference 1-D model. In order to test the adequacy of the latter we investigate if the observation geometry and inversion code are able to retrieve a synthetic model with a vertical boundary similar to the one found here. We choose as synthetic structure a 6-km sized cube with a 20% positive anomaly (Figure 2e). Since its shape and amplitude are well reconstructed, as illustrated by an E-W vertical cross section through the northern half of the cube in Figure 2f, we can consider that the vertical edge of the high-V_p body found from the observed data (Figure 2d) is a trustworthy feature.

In the inversion of the observations (Figure 2d, displaying the E-W cross section of V_p deviation at km 4178 N (northing in the kilometric UTM coordinate system)) the anomaly of the high-V_p body reduces amplitude at around 4 km bsl, whereas at its eastern edge the spread function value increases to above 1.5. Then it builds up again as a deeper high-V_p body reaching from 6 km bsl to the bottom of the inverted volume at 12 km bsl. It can be considered well resolved only down to 9 km bsl, as indicated by the 1.5 contour. The existence of the shallow high-V_p body above the basement, i.e., above 6 km bsl, is constrained by RAST, for which the ray paths are confined to above this level. While the local earthquake data allow a sampling to larger depth, this gets sparser with depth because of the distribution of the hypocenters. Therefore, even if the spread function value is under 1.5, the deeper high V_p in the LET inversion might then, in part, not be real but might result from leakage from the shallow high-V_p body documented by RAST and LET. The synthetic test displayed in Figure 2f shows the amount of smearing and the gradual decrease toward depth in the reconstruction of a shallow high-V_p cube. Within the same well-sampled region inside the 1.2–1.5 contour the inversion of the observations (Figure 2d) shows a shape different from that of the high-V_p anomaly, with a local decrease toward depth followed by an increase. The latter, deep high V_p should then be considered as a trustworthy structure, since it does not appear in the inversion of the synthetics and hence is not due to leakage from the shallow high V_p. This makes a case for a likely intracrustal root to the high-V_p body through the whole volume, which is resolved down to the bottom of the inverted domain at 12 km bsl. The absolute location in plane of such a column of material of magmatic origin inside the crust is not well constrained because it depends on the location computed for the deepest earthquakes that illuminate it. This is not well constrained in plane because of the reduced aperture of the array and the large heterogeneity.

The present V_p tomography allows estimation of the reliability and accuracy of the image of the high-V_p body found by *Hirn et al.* [1991] and sharpening of its 3-D shape. It confirms the extent in depth, well-constrained from above the basement around 5 km bsl, then reaching through the sedimentary cover with a broad extent at 2 km bsl and up to sea level. It constrains as well its location at the southern edge of the Valle del Bove and also under part of the summit region. Some of these elements have not been retrieved in other tomographies [*Cardaci et al.*, 1993; *De Luca et al.*, 1997; *Villaseñor et al.*, 1998]. Several interpretations have been based on the first-order characteristics, location, depth, size, and shape of the high-V_p body suggested by *Hirn et al.* [1991], which are still valid. The high-V_p body may represent an ensemble of fossil magma chambers of previous volcanoes whose position migrated [*Hirn et al.*, 1991]. In this geometry the absolute migration could have been that of the sedimentary and effusive cover of the V_p body toward the SE in the evolutionary model of Etna's shallow structure [*Borgia et al.*, 1992], rather than the migration to the NW of the magma feeding these volcanoes. The intrusion of the body may be related to the extensional context, as well as the excess amount of degassing with respect to erupted lava [*Hirn et al.*, 1997]. More specifically, because the shallow position of its top [*Laigle and Hirn*, 1999] is consistent with SO_2 exsolution depth [*Allard*, 1997], this body could be where the degassed unerupted magma is stored. Its deeper edge could be the origin for shallow magma transport, as in the models of *Dobran and Coniglio* [1996].

With the large amount of reliable S wave readings due to the use of three-component sensors, we can simultaneously invert for deviations of V_p and for V_p/V_s. When comparing the corresponding maps at 2 km bsl in Plates 2a and 2b within well-sampled areas, the striking features are as follows: (1) the low-V_p medium in which the high-V_p massive body is embedded has high V_p/V_s, which is consistent with its interpretation as a sedimentary domain, with water-filled pores and cracks, and (2) V_p/V_s variations show a smaller spatial wavelength within the massive high-V_p body, revealing regions of high V_p/V_s inside or at the edges of this body of intrusive magmatic origin, which could indicate the presence of a molten fraction in the solidified intrusion.

The threshold of the resolution spread function for V_p/V_s can be deduced from that of V_p by comparing the averaging vectors for the two parameters in the full-resolution matrix or the distributions of their spread function versus derivative weight sum, following *Toomey and Foulger* [1989]. This leads to a definition of a larger value for the threshold for V_p/V_s. The corresponding contours of 1.5 for good and 2 for acceptable sampling encompass smaller regions than the 1.2 and 1.5 contours for V_p, which is expected since the S wave data coverage is less dense.

In order to test the resolving power within that well-sampled region and the reliability of small size features in V_p/V_s with respect to those of V_p, we have to check that these particular spots are not the result of artifacts of the experiment. This could occur, for instance, from the data geometry, since the ray coverage for *S* waves is still poorer than that of *P* waves. A synthetic model is built by taking the 3-D V_p heterogeneity recovered from the inversion of observations and a constant V_p/V_s in space. The 3-D V_p heterogeneity and an almost null V_p/V_s deviation, which therefore is not shown because the image is almost blank, are easily retrieved. This test supports the conclusion that the heterogeneous features of V_p/V_s in the resulting model do not come from experimental or processing artifacts but presumably come from the real structure.

The complementary test is to check that a real structure with the small size of V_p/V_s anomalies resulting from the inversion of observations is within the effective resolving power of observations. We specifically build the synthetic model to be like the one retrieved from observations in both V_p and V_p/V_s. From the comparison of the results of the inversion of these synthetics (Plate 2 and Figures 3c and 4c) with the inversion of the observations (Plate 2 and Figures 3b and 4b), we can accept as trustworthy the regions where the two images are similar. This is, however, only true when they are similar in a well-sampled region, not when they are similar because of lack of sampling. The contour of the resolution spread function is superimposed in order to show where the results should be disregarded since they are outside the threshold of significance. It is obvious that the observed-synthetic image pairs have several features in common in the central part, where we may discuss V_p and V_p/V_s together and attempt an interpretation.

4. V_p/V_s Compared With V_p: Physical State of the Intrusive Magmatic Substructure of Etna

Seismic velocities are known to depend on a wide array of parameters: nature of the rock, temperature and pressure, phase changes in the material, porosity or crack distribution and shape, and nature and state of fluid content. These parameters cannot be uniquely derived from the measure of the spatial variation of deviations of V_p which mainly mirrors lithology, the distribution of rock types. Here V_p/V_s is also obtained, which by comparison with V_p allows discussion of defects, pores, and cracks and their fluid content. In the sediments, V_p is low and V_s is relatively even lower because of lithology, pores, and water content, so that V_p/V_s is relatively very high. We are most interested in the high-V_p parts because they mark the intrusive magmatic parts of the structure, in contrast to the low V_p of both the sedimentary material and the eruptive products of the volcano edifice. These intrusives with high V_p have also high V_s. Their V_p/V_s appears normal to lower than average because they are massive with respect to the surroundings which have low V_p and V_s but high V_p/V_s because they are made of more porous, loose, and water-filled sediments or eruptive products. Then those regions which have a high V_p/V_s within the high-V_p intrusive part are of particular significance because they correspond to low V_s, i.e., fluids containing fractured medium. Such volumes will hereinafter be called anomalies, and we tentatively interpret them as marking zones of transport, advection, and crystallization of molten fractions. However, at shallow depth, water may be the fluid involved rather than melt if temperature was low and V_p was not too high.

Tentatively, we identify and discuss five such anomalies on the maps at 2 km bsl of Plate 2. Anomaly 1 is located at 2 km bsl, SW of the Central Craters, where the edge of the high-V_p body is invaded locally by high V_p/V_s. Anomaly 2, just NE of the Central Craters, is also centered on 2 km bsl, where a high-V_p/V_s zone encroaches the northeastern edge of the generally low-V_p/V_s, high-V_p body. Anomaly 3 is the extension of anomaly 2 toward the surface to the south of the Central Craters by a contorted path. Anomaly 4 may extend anomaly 2 at depth from NE to SE of the central craters, where it might possibly link to the west with anomaly 1. Anomaly 5 is farther away from the summit, to the SE of the southern rim of Valle del Bove (km 506 E, km 4171 N), where a slightly high V_p/V_s coincides with the rather high V_p at the SE edge of the body.

Anomaly 1 is at 2 km bsl, where both V_p and V_p/V_s maps (Figures 3a and 3b) show a sharp boundary striking N-S just southwest of the Central Craters. However, the precise location of this limit differs on the two maps by at least a grid point (2 km). This can be considered as significant in this best sampled region, as suggested by the reconstruction in the synthetic test shown in the third column of Plate 2 and Figures 3 and 4. At location km 498 E, km 4174 N to km 4176 N in Figure 3, the edge of the high-V_p body to the east of this limit appears invaded by the high-V_p/V_s anomaly, whereas farther west the latter is instead associated with the low-V_p sediments. This anomaly is clearly seen in Figures 4a and 4b in the E-W cross sections at km 4174 N and km 4176 N. In the original tomography with 1984 data [*Hirn et al.*, 1991] a low V_p under the high V_p here was suggested as an example of the possible signature of a batch of magma, in a region where magma-sediment interaction would be likely from geochemical studies. During the preparation or initial phase of the 1991–1993 eruption, measurements of GPS and tilt and electronic distance measurements (EDM) showed deflation to have occurred in the region of anomaly 1. Indeed, the location in space and depth of the centers of deformation modeled from these measurements by *Nunnari and Puglisi* [1994a, 1994b] and *Bonnacorso et al.* [1994] coincide with anomaly 1, though they may be nearer to the summit according to *Bonnacorso* [1996].

Anomaly 2 is a high-V_p/V_s region that encroaches into the sharp and straight northeastern edge of the large high-V_p body seen at 2 km bsl in Plate 2a, southward along km 502 E (Plate 2b, see also Figures 4a and 4b on the N-S section at 502 E). This shows that a part of the high-V_p body has low V_s. It may be regarded as a part of the intrusive body, which is fractured and possibly contains magmatic fluids. The result of the synthetic test illustrates that the experiment is able to reconstruct such a feature. We may remark that its northern edge at 4 km beneath the surface is located at km 4180 N, beneath the NE rift zone of the 1865, 1928, 1971, and 1979 eruptions of Etna [*Chester et al.*, 1985]. These eruptions have had high output rates. The high-V_p/V_s anomaly could indicate a suitable structure for storing magma intermittently and for providing an efficient eruptive source when tapped. This can occur as a result of tectonic disruption at the top, which is likely the case for some of these eruptions, which occurred after episodes of surface fracturing between the summit and their vents on the NE flank. In recent periods of increased seismic monitoring, this region of anomaly 2 at km 4178 N, km 502 E has been revealed to be seismically activated in temporal relation to volcanic activity, while the effusive vents were ~3 km farther south. For instance, strong swarms of earthquakes occurred at the very end of the SE crater eruption of 1984 [*Hirn et al.*, 1991]

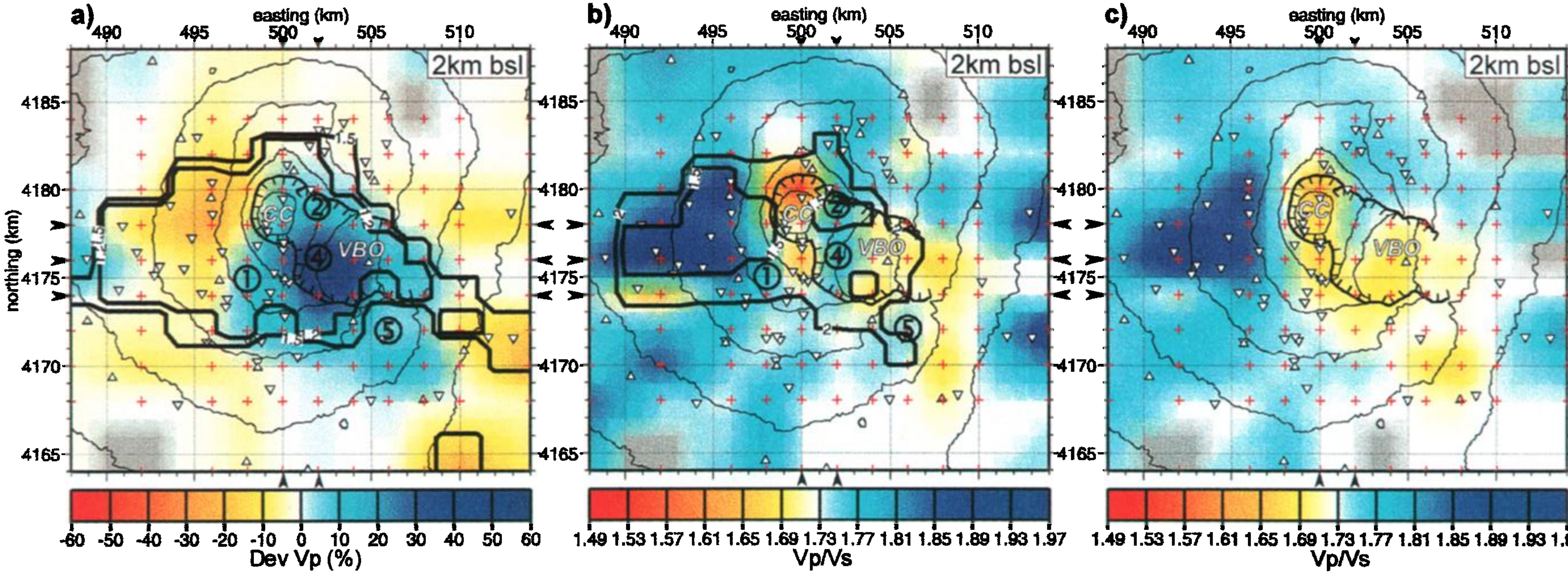

Plate 2. Map views at 2 km bsl. A curved barbed line includes the Valle del Bove (VBO) depression of the upper eastern flank and the Central Craters (CC) to its northeast. Labels 1, 2, 4, and 5 locate corresponding anomalies discussed in text; anomaly 3 is shallower and is located in the cross sections of Figures 3 and 4. (a) V_p deviation inverted from observations, superimposed are contours of values of 1.2, inner contour, and 1.5, outer contour, of the resolution spread function. (b) V_p/V_s inverted from observations, superimposed are contours of values of 1.5, inner contour, and 2, outer contour, of the resolution spread function for that parameter, (c) V_p/V_s inverted from times computed through synthetic model similar to that inverted from observations.

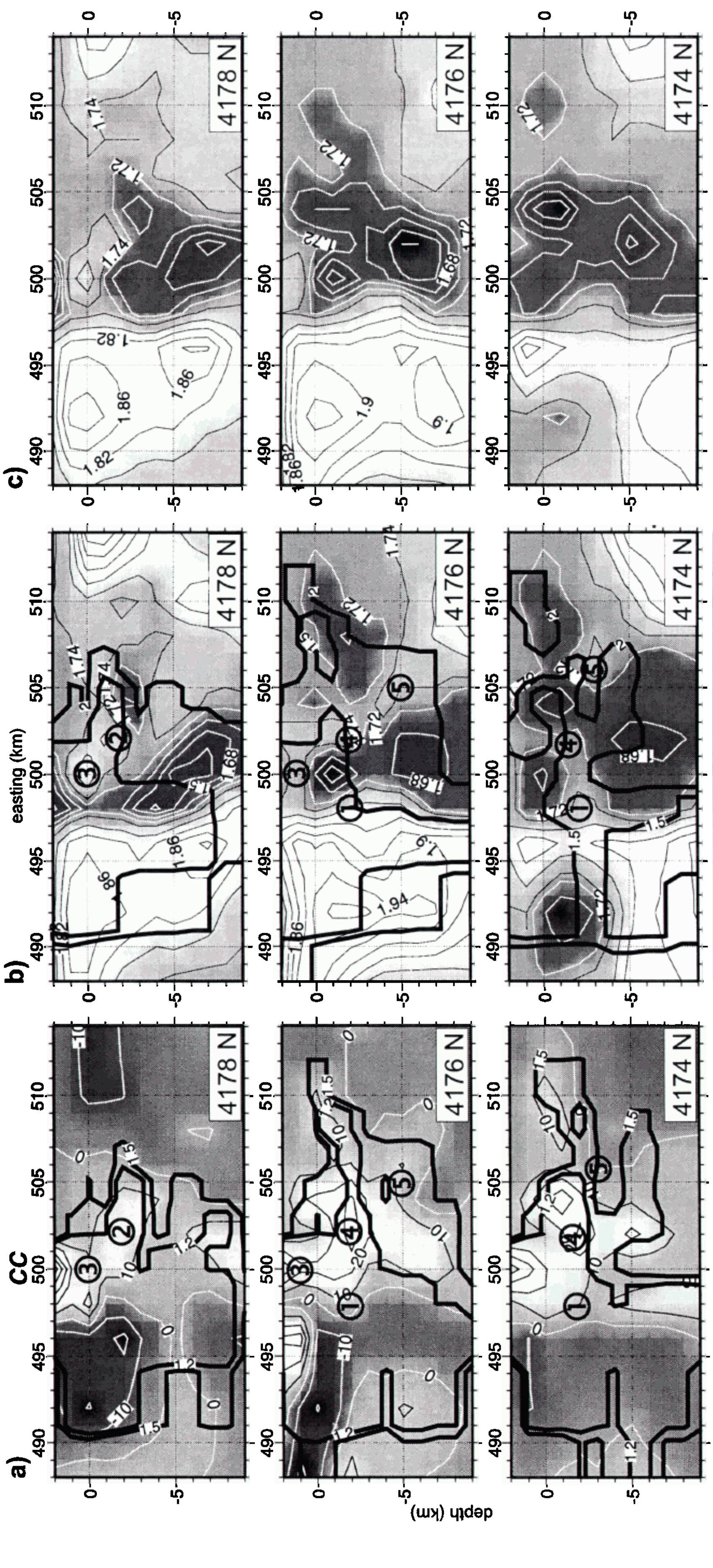

Figure 3. E-W cross sections at UTM kilometric northing (latitude) indicated at bottom right corner of each, with easting (longitude) kilometric ticks. Thick contours as in Plate 2. (a) V_p deviation inverted from observations, contours in percent, (b) V_p/V_s inverted from observations, and (c) V_p/V_s inverted from synthetic times computed through model similar to that inverted from observations.

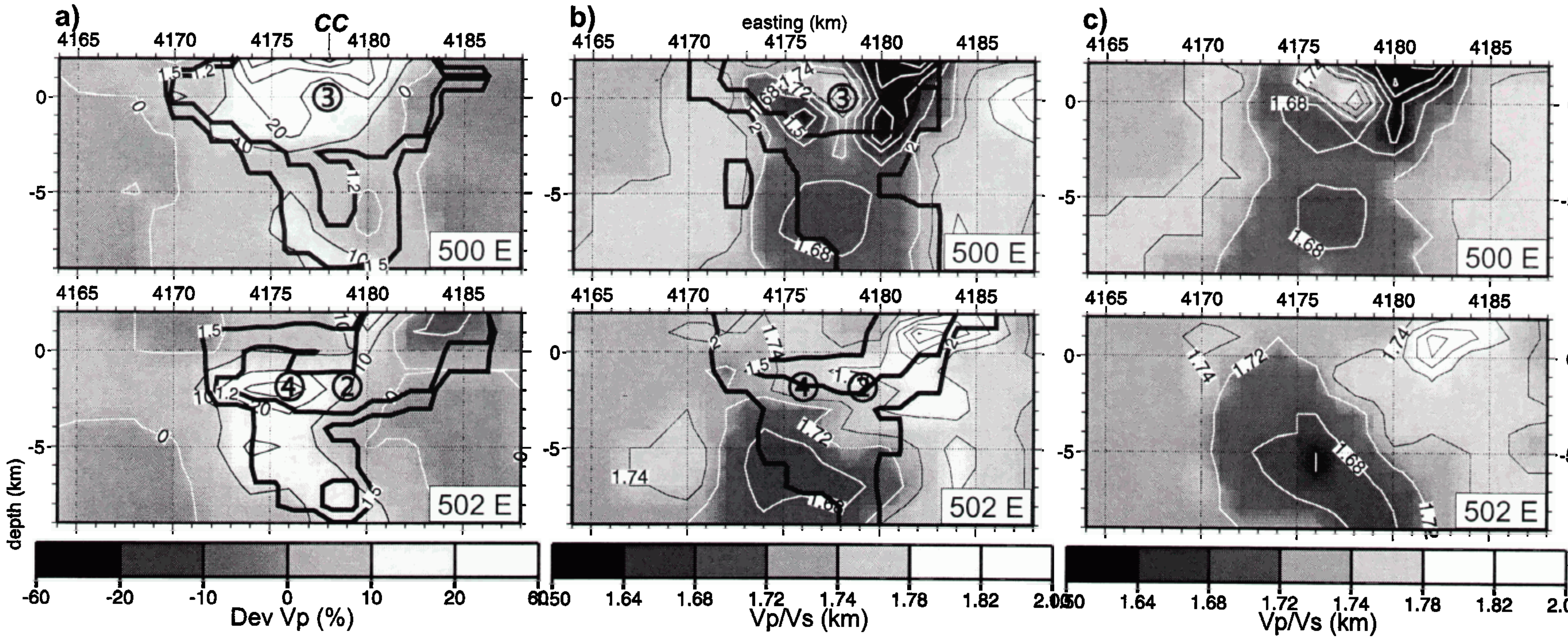

Figure 4. N-S cross sections at UTM kilometric easting (longitude) indicated at bottom right corner of each, with northing (latitude) kilometric ticks. Thick contours as in Plate 2. (a) V_p deviation inverted from observations, (b) V_p/V_s inverted from observations, and (c) V_p/V_s inverted from synthetic times computed through model similar to that inverted from observations.

and is also reported for the onset in December of the 1991–1993 eruption [*Ferrucci and Patanè*, 1993]. During the latter eruption the peculiar seismicity made of long-period events also developed in this region NE and close to the summit craters after January 1992 [*Falsaperla et al.*, 1994]. A new magma batch is shown by geochemistry to have mixed with previous ones [*Treuil and Joron*, 1994] in the second half of this eruption. Synthetic aperture radar (SAR) satellite-based deformation measurements during this second part were interpreted by *Massonnet et al.* [1995] as being due to magmatic discharge from a center of deflation that they locate slightly east of the Central Craters.

Anomaly 3 is suggested to be a physical link between anomaly 2, the site of seismic activation in the eruptive episodes described, and the corresponding surface vents. In the major 1991–1993 eruption, anomaly 2 was seismically activated, whereas venting did not occur above it but occurred in the southern summit region of the central cone. Also, while the 1984 eruption occurred at the vent of the southeast crater, the seismic swarms that marked its end occurred to the northeast of the summit, in anomaly 2. In the E-W section at km 4178 N (Figure 3), anomaly 2 at km 502 E (2 km bsl) is seen to be continued upward to the west, reaching sea level at 500 E. We identify this continuation as anomaly 3, for which a further upward continuation is shown in Figures 4a and 4b, in the N-S section which cuts at km 500 E just across the summit. There the anomalous, high-V_p and high-V_p/V_s volume shallows southward and finally reaches the surface along km 4173–4175 N, km 500 E. This corresponds broadly to the location of the vents of the 1991–1993 eruption and numerous previous eruptions of Etna. The synthetics suggest that this structure is trustworthy, although it is small. This is presumably because it is shallow and rather well sampled by the large number of temporary stations located on the upper flanks and Central Craters and of seismic sources in the region of anomaly 2.

Anomaly 4 is a southward extension of anomaly 2, east of the craters, at km 502 E on the map at 2 km bsl (Plate 2a). In the inversion of the observations (Plate 2b and Figure 4b), anomaly 4, with high V_p/V_s, reaches southward to km 4173 N, south of the craters and continues toward west (E-W cross sections at km 4174 N south of the Central Craters in Figures 3a and 3b). There anomaly 4 could connect as a faint anomaly of high V_p/V_s through the low-V_p/V_s and high-V_p body to the southern end of anomaly 1, situated a few kilometers SW of the Central Craters. Anomaly 4 would thus link anomaly 1 at distance with anomaly 2 east of the Central Craters. However, the corresponding synthetics show that the suggestion of anomaly 4 extending south of km 4176 N is not reliably established. Anomaly 4 could provide the structural link needed to be able to interpret the succession in time of events separated in space at the beginning of the 1991–1993 eruption. Indeed, this long-lasting eruption has been fed by a succession of compositionally different magma batches that followed diverse space-time paths toward eruption according to the geochemical studies of *Armienti et al.* [1994] and *Treuil and Joron* [1994]. The latter describe the succession with time as (1) a mingling of two different batches from the very beginning of the eruption on December 14, 1991, (2) evolution to a more stationary flux of heterogeneous mix from January to April 1992, and (3) the arrival of a new batch, visible from May 1992 and increasing in proportion with time. Deflation in the vicinity of anomaly 1 occurred before or in the early part of the eruption. Anomaly 1 might, in this case, have provided the pressure or material to feed one of the diverse sources of magma to this eastern slope of the summit above Valle del Bove where lava vented, through anomalies 4 and 2, and then through anomaly 3. Such a scheme is supported by evidence from the migration of seismicity along part of the path, since a migration is reported to have occurred from the SE toward the Central Craters during the preeruptive seismic swarm at Etna on December 14, 1991 [*Ferrucci and Patanè*, 1993; *Alparone et al.*, 1994].

Anomaly 5 is located at the southeastern edge of the intrusive magmatic body, follows outside the SE rim of Valle del Bove, and extends eastward to km 506 E, km 4172 N in the inversion of observed data but is more subdued and less continuous in the synthetics. Also, the resolution spread function is about at the threshold value of significance. In this SE region, there are historical flank lava flows like those from Monte Ilice and Monterosso. This coincidence might not be fortuitous. Indeed, most other lower flank eruptions are essentially aligned with and related to the Etna rift zones to the north, south, and southwest, but these are not. Instead, they would appear to be related to an anomaly at depth. This is similar to the case of the eruptions on the NNE flank, which occur above anomaly 2 where it reaches the NE edge of the intrusive body, as mentioned in anomaly 2 description.

Anomalies 2 and 5 share another spatial coincidence with the recent larger superficial earthquakes of Etna. Anomaly 2, NE of the summit, where it reaches the edge of the high-V_p body (Figure 2), is the site of the posteruptive, October 17, 1984, and later repeating shallow destructive earthquakes known from location names as Piano Provenzana or Pernicana events. Similarly, anomaly 5 to the ESE of Etna reaches the edge of the high-V_p body (Figure 2) near towns after which the posteruptive, shallow destructive earthquakes are known, which occurred on October 18, 1984, at Zafferana and October 29, 1984, at Fleri. These three shallow flank earthquakes occurred at the cessation of venting near the summit, a relation shown to be statistically significant through the record of historical eruptions and earthquakes [*Nercessian et al.*, 1991]. They are not only in the periphery of the magmatic domain of Etna [*Hirn et al.*, 1991] but are also above anomalies that are suggested by the present tomography to contain a proportion of melt and to be structurally connected to each other and to the summit. The time and space relations suggest a causal link or common activation, and these earthquakes appear to be coupled to magmatic activity, even if they are in the upper and peripheral zone of the volcano where flank instability could be invoked. In fact, *Patanè et al.* [1994] contend that focal mechanisms do not agree with the latter model and also that their diversity does not allow them to interpret them as due to a uniform regional stress. The orientations of dip slip that they find for these shocks NE and ESE of Etna appear to be conjugate when considered with respect to the high-V_p intrusive core of the volcano in between. This suggests that these earthquakes could be interpreted in terms of a bulk westward subsidence of the high-V_p block, as a transient marking the end of the sustained magma pressure which fed the eruption.

5. Discussion and Conclusions

The present V_p and V_p/V_s tomography uses a data set of Etna local earthquakes recorded by a dense array temporarily deployed in 1984 [*Hirn et al.*, 1991] augmented by data of recent similar deployments in 1994 and 1995, which included stations in the region of the Valle del Bove. Velocity constraints on the upper part of the model are provided by new artificial source data and inversions for the minimum 1-D model from two end-member initial models. In spite of the change of the velocity model and of the inversion code the same structure is found as in the original tomography, where the results were deemed reliable. This is likely due to the dense array character of the data. The present results extend and sharpen those of the original tomography, confirming the high-V_p body centered on the southern Valle del Bove and reaching up toward sea level that was revealed by the original tomography of *Hirn et al.* [1991]. In contrast, images resulting from other studies with more data but a sparser array were reported to differ from the original one [*Cardaci et al.*, 1993; *De Luca et al.*, 1997; *Villaseñor et al.*, 1999], but they also differ from each other, although the bulk of their database is the same. In our case of the dense array the information on structure appears robust with respect to the velocity model or inversion code. Images obtained from sparse arrays instead appear code- and assumption-dependent. This hampers interpretation in very heterogeneous volcanic areas.

The present LET retrieves the high-V_p body which reaches to shallow depth, being best expressed at 2 km bsl and even shallower. This shallow depth range is the region where the results differ most among the different published LET studies of Etna. The waves turned back by the basement in the RAST [*Laigle and Hirn*, 1999] exclusively sample this shallow part. They hence constrain the high-V_p body to extend to shallow depth. This demonstrates the reliability of the present LET as well as of the original one [*Hirn et al.*, 1991], which found this feature, whereas other LET do not find it at this depth. Synthetic tests are performed to check the quality of the LET inversion and to define trustworthy regions of the inverted volume. These synthetic tests are compared with indicators extracted from the full-resolution matrix. The areas not well reconstructed in the synthetics have resolution indicators below the threshold calibrated by *Laigle and Hirn* [1999] from the consistency between results of LET and RAST, two tomographies with completely different geometry.

The high-V_p body resulting from the inversion of the observations can be regarded as an acceptable representation of the real structure, since synthetic tests show that the shape of its edge comes from information in the data and not from the experiment geometry or inversion code. Similarly, synthetics establish that its vertical extension as a sharp contrast in velocity could be correctly retrieved in spite of the assumption of an initial 1-D velocity-depth model. LET establishes the presence of a deeper high-V_p anomaly, which traverses the crust below the top of the basement and which is possibly the root of the large high-V_p body embedded in the sediments.

The likely intrusive magmatic nature of the high-V_p body is indicated by the contrast of its velocity with that of surrounding sediments. Then the exceptional proportion of reliable shear wave readings from three-component sensors provides the data to discuss its physical state. When considering V_p/V_s, the massive high-V_p body appears significantly heterogeneous, and complementary synthetic tests establish that this is required by the data. Regions inside it where V_s is low can then be suspected of containing a proportion of melt or being fractured and acting as pressure links or transport zones. A main such anomaly is imaged at 2 km bsl east of the Central Craters. Seismic activation occurred there in relation with eruptive phenomena at surface vents located south of the Central Crater, such as the stopping phase of the 1984 eruption and an episode of the 1991–1993 eruption. Indeed, LET resolves a contorted structural anomaly linking this deep anomaly east of the Central Craters below sea level and the region of the surface vents located south of them. The main anomaly inside the high-V_p body east of the Central Craters may also connect to the edge of this high-V_p body. This is the case, for instance, toward the north, where it reaches the region of the NE rift zone. Flank eruptions occurred nearby, as well as destructive earthquakes in relation to eruptive episodes. Another anomaly is located at 2 km bsl under the SW edge of the high-V_p body. It corresponds to the location of a deflation source in the preparation or initial phase of the 1991–1993 eruption. However, venting occurred far away, on a fissure radiated from the summit, after a preeruptive seismic crisis, which migrated from the SE to the summit. A connection at depth between these zones to the south between the anomalies SW and east of the Central Craters is suggested in the inverted structure but is only marginally significant using the available data.

By taking into account the heterogeneities in structure and physical state retrieved by seismic tomography, a succession of seismic events, deformational episodes, and geochemical variation of lava can be put in a consistent perspective with respect to recent eruptions. Some of the structural features had been detected and discussed previously but here are brought into focus. Better resolution by more extensive and dense spatial sampling is still desirable. It is within reach of experimental efforts of simultaneous deployment of a large number of three-component seismographs, up the volcano and inside the Valle del Bove for a long duration to record a larger set of well-distributed earthquakes.

Acknowledgments. This research is part of the multimethod seismic approach of Etna funded partly by EC Environment Programme, Volcanic Hazard, under contract ETNASEIS EV5V-CJ92-0187 to A. Hirn, R. Nicolich, J. Gallart, and B. Brandsdottir. The help of E. Kissling and J. Ansorge of ETH Zurich in providing additional instruments is acknowledged. We acknowledge the use of Simulps14 and TOMO2GMT packages of E. Kissling, F. Haslinger, and S. Husen. We thank C. Thurber, J. Hole, and anonymous referees for extensive and constructive criticism and suggestions which led to significant evolution of the paper and for their patience. Contribution IPGP 1684.

References

Accaino, F., M. Romanelli, L. Petronio, L. Cernobori, M. Laigle, and ETNASEIS Group, Etna: Refraction and near vertical seismic reflection data on the volcanic edifice, in *The European Laboratory Volcanoes*, edited by R. Casale et al., pp. 421–429, Eur. Commun., Luxenbourg, 1998.

Allard, P., Endogenous magma degassing and storage at Mount Etna, *Geophys. Res. Lett.*, *24*, 2219–2222, 1997.

Alparone, S., O. Pellicori, A. Ursino, F. Ferrucci, S. Gresta, and I. Guerra, Shallow microseismic swarms and intrusive mechanisms at Mount Etna: 1989–1991, *Acta Vulcanol.*, *4*, 75–79, 1994.

Armienti, P., M. T. Pareschi, F. Innocenti, and M. Pompilio, Effects of magma storage and ascent on the kinetics of crystal growth: The case of the 1991–93 Mt Etna eruption, *Contrib. Mineral. Petrol.*, *115*, 402–414, 1994.

Benz, H. M., B. A. Chouet, P. B. Dawson, J. C. Lahr, R. A. Page, and J. A. Hole, Three-dimensional *P* and *S* wave velocity structure of Redoubt Volcano, Alaska, *J. Geophys. Res.*, *101*, 8111–8128, 1996.

Bonaccorso, A., Dynamic inversion of ground deformation data for modelling volcanic sources (Etna 1991–93), *Geophys. Res. Lett.*, *23*, 451–454, 1996.

Bonaccorso, A., R. Velardita, and L. Villari, Ground deformation modelling of geodynamic activity associated with the 1991–93 Etna eruption, *Acta Vulcanol.*, *4*, 87–96, 1994.

Borgia, A., L. Ferrari, and G. Pasquarè, Importance of gravitational spreading in the tectonic and volcanic evolution of Mount Etna, *Nature*, *357*, 231–235, 1992.

Cardaci, C., M. Coviello, G. Lombardo, G. Patanè, and R. Scarpa, Seismic tomography of Etna volcano, *J. Volcanol. Geotherm. Res.*, *56*, 357–368, 1993.

Catalano, R., P. Di Stefano, A. Sulli, and F. P. Vitale, Paleogeography and structure of the central Mediterranean: Sicily and its offshore area, *Tectonophysics*, *260*, 291–323, 1996.

Chester, D. K., A. M. Duncan, J. E. Guest, and C. R. J. Kilburn, *Mount Etna: The Anatomy of a Volcano*, 404 pp., Chapman and Hall, New York, 1985.

Dawson, P. B., B. A. Chouet, P. G. Okubo, A. Villaseñor, and H. M. Benz, Three-dimensional velocity structure of the Kilauea caldera, Hawaii, *Geophys. Res. Lett.*, *26*, 2805–2808, 1999.

De Luca, G., L. Filippi, G. Patanè, R. Scarpa, and S. Vinciguerra, Three-dimensional velocity structure and seismicity of Mt Etna volcano, Italy, *J. Volcanol. Geotherm. Res.*, *79*, 123–138, 1997.

Dobran, F., and S. Coniglio, Magma ascent simulations of Etna's eruptions aimed at internal system definition, *J. Geophys. Res.*, *101*, 713–731, 1996.

Eberhart-Phillips, D., Local earthquake tomography: Earthquake source regions, in *Seismic Tomography: Theory and Practice*, edited by H. M. Iyer and K. Hirahara, pp. 613–643, D. Reidel, Norwell, Mass., 1993.

Evans, J. R., D. Eberhardt-Phillips, and C. H. Thurber, User's manual for SIMULPS12 for imaging V_p and V_p/V_s: A derivative of the Thurber tomographic inversion SIMUL3 for local and explosions, *U.S. Geol. Surv. Open File Rep.*, *94-431*, 101 pp., 1994.

Falsaperla, S., E. Privitera, S. Spampinato, and C. Cardaci, Seismic activity and volcanic tremor related to the December 14, 1991 Mt Etna eruption, *Acta Vulcanol.*, *4*, 63–73, 1994.

Ferrucci, F., and D. Patanè, Seismic activity accompanying the outbreak of the 1991–1993 eruption of Mt Etna (Italy), *J. Volcanol. Geotherm. Res.*, *57*, 125–135, 1993.

Hirn, A., A. Nercessian, M. Sapin, F. Ferrucci, and G. Wittlinger, Seismic heterogeneity of Mt Etna: Structure and activity, *Geophys. J. Int.*, *105*, 139–153, 1991.

Hirn, A., R. Nicolich, J. Gallart, M. Laigle, L. Cernobori, and ETNASEIS Scientific Group, Roots of Etna volcano in faults of great earthquakes, *Earth Planet. Sci. Lett.*, *148*, 171–191, 1997.

Humphreys, E., and R. W. Clayton, Adaptation of back projection tomography to seismic travel time problems, *J. Geophys. Res.*, *93*, 1073–1085, 1988.

Kissling, E., Geotomography with local earthquakes, *Rev. Geophys.*, *26*, 659–698, 1988.

Kissling, E., W. L. Ellsworth, D. Eberhart-Phillips, and U. Kradolfer, Initial reference models in local earthquake tomography, *J. Geophys. Res.*, *99*, 19,635–19,646, 1994.

Laigle, M., Images sismiques de l'Etna à diverses échelles: Nouveaux éléments sur son comportement et le cadre régional, Ph.D. thesis, 288 pp., Univ. of Paris 7, Paris, 1998.

Laigle, M., and A. Hirn, Explosion-seismic tomography of a magmatic body beneath Etna: Volatile discharge and tectonic control of volcanism, *Geophys. Res. Lett.*, *26*, 2665–2668, 1999.

Laigle, M., L. Petronio, M. Romanelli, F. Accaino, and ETNASEIS Group, Etna: Data of cross-volcano seismic transmission, in *The European Laboratory Volcanoes*, edited by R. Casale et al., pp. 431–441, Eur. Commun., Luxembourg, 1998.

Lees, J. M., The magma system of Mount St Helens: Non-linear high resolution *P*-wave tomography, *J. Volcanol. Geotherm. Res.*, *53*, 103–116, 1992.

Lees, J. M., and R. S. Crosson, Tomographic inversion for three-dimensional velocity structure at Mount St. Helens using earthquake data, *J. Geophys. Res.*, *94*, 5716–5728, 1989.

Lévêque, J. J., L. Rivera, and G. Wittlinger, On the use of the checkerboard test to assess the resolution of tomographic inversion, *Geophys. J. Int.*, *115*, 313–318, 1993.

Massonnet, D., P. Briole, and A. Arnaud, Deflation of Mount Etna monitored by spaceborne radar interferometry, *Nature*, *375*, 567–570, 1995.

Menke, W., *Geophysical Data Analysis: Discrete Inverse Theory*, 260 pp., Academic, San Diego, Calif., 1984.

Nercessian, A., A. Hirn, and M. Sapin, A correlation between earthquakes and eruptive phases at Mt Etna: An example and past occurrences, *Geophys. J. Int.*, *105*, 131–138, 1991.

Nercessian, A., A. Hirn, J. C. Lépine, and M. Sapin, Internal structure of Piton de la Fournaise volcano from seismic wave propagation, *J. Volcanol. Geotherm. Res.*, *70*, 125–143, 1996.

Nicolich, R., M. Laigle, A. Hirn, L. Cernobori, and J. Gallart, Crustal structure of the Ionian margin of Sicily: Etna volcano in the frame of regional evolution, *Tectonophysics*, in press, 2000.

Nunnari, G., and G. Puglisi, The global positioning system as a useful technique for measuring ground deformations in volcanic areas, *J. Volcanol. Geotherm. Res.*, *61*, 267–280, 1994a.

Nunnari, G., and G. Puglisi, Ground deformation studies during the 1991–1993 Etna eruption using GPS data, *Acta Vulcanol.*, *4*, 101–107, 1994b.

Ohmi, S., and J. M. Lees, Three-dimensional *P*- and *S*-wave velocity structure below Unzen volcano, *J. Volcanol. Geotherm. Res.*, *65*, 1–26, 1995.

Okubo, P. G., H. M. Benz, and B. A. Chouet, Imaging the crustal magma source beneath Mauna Loa and Kilauea volcanoes, *Geology*, *25*, 867–870, 1997.

Patanè, G., A. Montalto, I. Imposa, and S. Menza, The role of regional tectonics, magma pressure and gravitational spreading in earthquakes of the eastern sector of Mt Etna volcano (Italy), *J. Volcanol. Geotherm. Res.*, *61*, 253–266, 1994.

Rowan, L. R., and R. W. Clayton, The three-dimensional structure of Kilauea volcano, Hawaii from travel time tomography, *J. Geophys. Res.*, *98*, 4355–4375, 1993.

Selvaggi, L., and C. Chiarabba, Seismicity and *P*-wave velocity image of the southern Tyrrhenian subduction zone, *Geophys. J. Int.*, *121*, 818–826, 1995.

Sharp, A. D. L., P. M. Davis, and F. Gray, A low velocity zone beneath Mount Etna and magma storage, *Nature*, *287*, 587–591, 1980.

Spakman, W., S. Stein, R. van der Hilst, and R. Wortel, Resolution experiments for NW Pacific subduction zone tomography, *Geophys. Res. Lett.*, *16*, 1097–1100, 1989.

Thurber, C. H., Earth structure and earthquake locations in the Coyote Lake area, central California, *J. Geophys. Res.*, *88*, 8226–8236, 1983.

Thurber, C. H., Seismic detection of the summit magma complex of Kilauea volcano, Hawaii, *Science*, *223*, 165–167, 1984.

Thurber, C. H., Local earthquake tomography: Velocities and V_p/V_s—Theory, in *Seismic Tomography: Theory and Practice*, edited by H. M. Iyer and K. Hirahara, pp. 563–583, D. Reidel, Norwell, Mass., 1993.

Toomey, D. R., and G. R. Foulger, Tomographic inversion of local earthquake data from the Hengill-Grensdalur central volcano complex, Iceland, *J. Geophys. Res.*, *94*, 17,497–17,510, 1989.

Treuil, M., and J. L. Joron, Etude géochimique des éléments en traces dans les laves émises au cours de l'éruption 1991–1993 de l'Etna: Mise en évidence des contributions de la source, de la fusion partielle, de la différentiation et des modalités de transfert des magmas, *Acta. Vulcanol.*, *4*, 29–45, 1994.

Um, J., and C. H. Thurber, A fast algorithm for two-point seismic ray-tracing, *Bull. Seismol. Soc. Am.*, *77*, 972–986, 1987.

Villaseñor, A., H. M. Benz, L. Filippi, G. De Luca, G. Patanè, R. Scarpa, and S. Vinciguerra, Three-dimensional *P*-wave velocity structure of Mt. Etna, Italy, *Geophys. Res. Lett.*, *25*, 1975–1978, 1998.

J. Diaz and J. Gallart, Institut de Ciencies de la Terra "Jaume Almera," CSIC, c/Lluis Sole Sabaris s/n, E-08028 Barcelona, Spain.

A. Hirn, M. Laigle, J.-C. Lépine, and M. Sapin, Laboratoire de Sismologie Expérimentale, Département de Sismologie, UMR 7580 CNRS, Institut de Physique du Globe, 4 Place Jussieu, F-75252 Paris Cedex 05, France. (hirn@ipgp.jussieu.fr)

R. Nicolich, Dipartimento di Ingegneria Navale del Mare i per l'Ambiente, Università di Trieste, Via Valerio 10, I-34127, Trieste, Italy.

(Received June 2, 1999; revised May 7, 2000;
accepted May 31, 2000.)